PCCP

Solvent Effects on the Intramolecular Conversion of Trimethylsulfonium Chloride to Dimethylsulfide and Methylchloride

Journal:	*Physical Chemistry Chemical Physics*
Manuscript ID:	CP-ART-09-2014-003965
Article Type:	Paper
Date Submitted by the Author:	04-Sep-2014
Complete List of Authors:	Lankau, Timm; National Tsing Hua University, Department of Chemistry Yu, Chin Hui; National Tsing Hua University, Chemistry

ARTICLE TYPE www. rsc.org/xxxxxx | XXXXXXXX

Solvent Effects on the Intramolecular Conversion of Trimethylsulfonium Chloride to Dimethylsulfide and Methylchloride†

Timm Lankau,[a] Chin Hui Yu[b]

Received Xth XXXXXXXXXX 20XX, Accepted Xth XXXXXXXXX 20XX
First published on the web Xth XXXXXXXXXX 200X
DOI: 10.1039/b000000x

The formation of CH_3Cl from $(CH_3)_3SCl$ in various solvents has been studied with M05/6-311+G(2d,p) DFT calculations to quantify the influence of the solvent on the stability of sulfonium cations. Four different pathways (one S_N1, one backside and two frontside attacks for S_N2) as well as the formation of different ion pairs (tripod, seesaw, and linear) are discussed to investigate the origin of the kinetic solvent effect (KSE) and the contribution of ion pairs to the overall reaction. Ion pairs are formed only in solvents with a permittivity ε smaller than 28, but the reaction proceeds *via* a standard S_N2 mechanism with a backside attack in all solvents. The formation of ion pairs does not change the order of the rate law, but it strongly influences the KSE, which can distinguish between reactions starting from the free ions and those starting from ion pairs, in contrast to standard kinetic analysis.

1 Introduction

Sulfonium cations (R_3S^+) play an important role in chemical and biological systems. Their chemical applications include the synthesis of oxiranes[1–4] and their biological applications range from herbicides[5] to dietary supplements and medications,[6,7] to name a few. Crucial for the production and storage[3–5,8–10] of sulfonium compounds is their reactivity in different environments. This work focusses on the stability of trimethylsulfonium chloride $(CH_3)_3S^+Cl^-$ in various solvents

$$[(CH_3)_3S^+]_{(sol)} + Cl^-_{(sol)} \longrightarrow (CH_3)_2S_{(sol)} + CH_3Cl_{(sol)} \quad (1)$$

to analyse the influence of the environment onto the conversion reaction.[11]

Among the first to analyse reaction 1 were Gleave *et al.*,[12] who reported a bimolecular mechanism for the conversion of $(CH_3)_3SOH$ and $(C_2H_5)_3SOH$ in water and a unimolecular one for $(CH_3)(i\text{-}C_3H_7)_2SOH$ and $(CH_3)_2(t\text{-}C_4H_9)SOH$. The effect of the anion was studied with the $(CH_3)_3S^+$ cation in absolute ethanol. A bimolecular reaction was reported for the OH^- and phenoxide anions while a unimolecular rate constant was reported for CO_3^{2-}, Br^- and Cl^-. This early work clearly showed the importance of the chemical environment for the reaction of sulfonium cations as the rate of the second-order solvolysis of $(CH_3)_3SOH$ in ethanol was more than 20000 times higher than that in water.

Further analysis of the kinetics of reaction 1 yielded different results for its molecularity depending on the moving group, the solvent, and other experimental conditions. The conversion of tribenzylsulfonium chloride in 90% acetone was reported to be of second order with a large salt effect.[13] A change of the solvent from water to ethanol in the first order solvolysis of trimethylsulfonium perchlorate[14] increased the rate just by a factor of 20. The analysis of the transition state showed that the breaking C···S bond became longer in the transition state if substituents supply electrons to the moving carbon atom.[14,15] Dimethyl sulfide and the benzyl halides are the only products reported for the conversion of benzyldimethylsulfonium salts in chloroform[16] which suggests that resonance stabilisation of the cation determines the moving group. It was found that the reaction is not exactly first order in concentration, but exactly first order in conductance. The proposed mechanism is neither standard S_N1 nor S_N2, but includes a triple ion containing two sulfonium and one halide ion. A bimolecular mechanism has been reported[11] for the reaction between the (4-methoxybenzyl)-dimethylsulfonium cation and nucleophiles of intermediate hardness (N_3^-, SO_3^{2-}, SCN^-), but not with hard (OH^-, Cl^-, OCN^-) or soft ones (CN^-, I^-), which suggests that no simple relationship exists between the chemical hardness of the nucleophile and the observed kinetics of reactions.

The solvolysis of various sulfonium salts R'_3SX in a series of solvents

† Electronic Supplementary Information (ESI) available: evaluation of the computational methods, additional graphics, an annotated list of all symbols, the computational setup for calculations with explicit water molecules, geometries, frequencies and energies of the discussed clusters, animation of the CRD path. See DOI: 10.1039/b000000x/

[a] *Department of Chemistry, National Tsing Hua University, 101 KuangFu Road Sec.2, Hsinchu 30013, Taiwan.*
[b] *Department of Chemistry, National Tsing Hua University, 101 KuangFu Road Sec.2, Hsinchu 30013, Taiwan. Fax: +886-(0)3-5721534; Tel: +886-(0)3-5162080; E-mail: chyu@oxygen.chem.nthu.edu.tw*

$$X^- + R'_3S^+ + ROH \longrightarrow R'_2S + R'OR + HX \qquad (2)$$

has been subjected to many kinetic investigations.[11,13–15,17–20] The solvolysis of dimethyl-*t*-butyl sulfonium halides $R_2R'SX$ and the role of ion pairs $R_2R'S^+ \cdot X^-$ in the solvolysis process

$$\text{prod} \longleftarrow R_2R'S^+ + X^- \overset{K_A}{\rightleftharpoons} R_2R'S^+ \cdot X^- \longrightarrow \text{prod}\,, \qquad (3)$$

where K_A is the equilibrium constant, has been studied in great detail.[17–21] The solvolysis proceeds *via* a solvent stabilised *t*-butyl cation[17] and the ion pair concentration increases as the permittivity of the solvent decreases. The value of K_A continuously decreases as the solvent becomes more polar, but is still greater than one for pure water.[18] The ion pair itself can be attacked by nucleophiles in solvents with a low permittivity,[19] but this reaction pathway only seems to be relevant for experiments with an excess of the nucleophile. The formation of ion pairs speeds up the solvolysis reaction in non-polar solvents.[20] In a series of solvolysis experiments using mixtures of water with N,N-dimethylformamide, ethanol, ethylene glycol and dioxane as solvents, the rate of solovolysis reactions decreases as the permittivity of a solvent increases. In contrast, the rate increases with the permittivity in mixtures of N-methylformamide and water. The failure of N-methylformamide to fit into the series of solvolysis experiments suggests that solvent-solute interactions cannot be neglected in the kinetics of solvolysis reactions.

A computational study of structural and thermodynamic properties of sulfonium ions[22] reported enthalpy changes for the transfer of the methyl group in the gas-phase in agreement with experimental data. However, the calculations failed to reproduce those for solutions. The influence of solvation effects on the transfer of the methyl group[23] was analysed by adding up to four water molecules in the calculation, but the calculated enthalpies for the methyl transfer from $(CH_3)_3S^+$ to $CH_3SCH_2CO_2^-$ (2-methylsulfanylacetate ion) still carried an error of more than 60 kcal/mol compared to experimental data. The chemical environment (vacuum, ethanol, and water) can be included into Hartree-Fock calculations *via* a generalized Born formula[24] to analyse reaction 1. The reported values of ΔE_{reac} *in vacuo* for Equation 1 vary between -502 and -569 kJ mol^{-1}. A linear ion pair was not observed for the gas phase reaction, but was found in ethanol and water. Although the formation of a non-linear ion pair was reported, its role in the methyl transfer reaction was not investigated. Later, B3LYP calculations on the non-linear $(CH_3)_3S^+ \cdot Cl^-$ ion pair were done as part of an analysis of ^{33}S NMR spectra of sulfonium salts.[25] The ion pair with the chloride ion coordinated by the hydrogen atoms of the methyl groups was found to be the most stable one; nevertheless, the predicted differences in the NMR properties of the ion pair and the free $(CH_3)_3S^+$ cation were too small to be verified by experiment.

This work examines the conversion of $(CH_3)_3SCl$ according to Equation 1 in various solvents to analyse the effect of the solvent on its mechanism. A special emphasis will be placed on the role of ion pairs in the mechanism of the conversion reaction as a function of the solvent. The possibility of alternative reaction paths involving CH_3^+ ions or a frontside attack and how the different paths manifest themselves in the macroscopic kinetics of the conversion reaction are analysed based on the calculated energies to complete this study.

2 Computational Setup

The evaluation of a suitable computational method for the analysis of the conversion of $(CH_3)_3SCl$ and related properties was done with two setups. The first one focuses on the properties[26] of $(CH_3)_2S$. Ten computational methods (HF, MP2, OLYP, OPBE, B3LYP, O3LYP, X3LYP, PBE1PBE, M05, M05-2X) and 12 basis sets [6-31G(d,p), 6-31+G(d,p), 6-31++G(d,p), 6-311G(d,p), 6-311+G(d,p), 6-311++G(d,p), D95+(d,p), D95++(d,p), cc-pVDZ, aug-cc-pVDZ, cc-pVTZ, aug-cc-pVTZ] as defined in the Gaussian 09 program package[27] were used. The geometry of the $(CH_3)_2S$ molecule was optimised in the vacuum under the constraint of C_{2v} symmetry followed by a normal mode analysis. The root σ_{tot} of the normalised and squared differences between the calculated values of the CS bond length (r_1), the average CH bond length (r_2), the CSC bond angle (ω_1), the average HCH bond angle (ω_2), the molecular dipole moment (μ), and the frequencies ($f_{1\ldots3}$) of the three low lying vibrational modes involving the sulfur atom and their experimental counterparts (r_i^{ref}, ω_i^{ref}, μ^{ref}, f_i^{ref})

$$\sigma_{\text{tot}} = \sqrt{\sum_{i=1}^{2}\left(\frac{\Delta r_i}{r_i^{\text{ref}}}\right)^2 + \sum_{i=1}^{2}\left(\frac{\Delta \omega_i}{\omega_i^{\text{ref}}}\right)^2 + \left(\frac{\Delta \mu}{\mu^{\text{ref}}}\right)^2 + \sum_{i=1}^{3}\left(\frac{\Delta f_i}{f_i^{\text{ref}}}\right)^2} \qquad (4)$$

was used to judge the 120 data sets (Section S.1. References to the ESI are indicated with a preceding 'S'.). These data showed that the M05 functional[28] either with the cc-pVDZ ($\sigma_{\text{tot}} = 0.0513$) or with the cc-pVTZ basis set ($\sigma_{\text{tot}} = 0.0594$) yields the best reproductions of the properties of $(CH_3)_2S$.

Next, the size of the basis set is systematically increased until convergence is observed in barrier height of the nucleophilic substitution reaction of dimethyl sulfide in the vacuum

$$(CH_3)_2S + Cl^- \longrightarrow CH_3S^- + CH_3Cl \quad . \qquad (5)$$

$(CH_3)_2S$ was used instead of $(CH_3)_3S^+$ for this evaluation, because a barrier had been observed in reaction 5 while no barrier had been reported for reaction 1. The M05 functional selected from the previous evaluation was paired with 13 basis sets [6-311G(d,p), 6-311G(2d,p), 6-311+G(d,p), 6-311+G(2d,p), 6-311++G(d,p), 6-311++G(2d,p), cc-pVDZ, cc-pVTZ, cc-pVQZ, cc-pV5Z, aug-cc-pVDZ, aug-cc-pVTZ,

solvent	ε	*cmf*
cyclohexane	2.0165	0.2531
carbon tetrachloride	2.228	0.2904
benzene	2.2706	0.2975
carbon disulfide	2.6105	0.3493
tetralin	2.771	0.3712
dibutyl ether	3.0473	0.4056
diethyl amine	3.5766	0.4620
diphenyl ether	3.73	0.4764
ethyl phenyl ether	4.1797	0.5145
anisole	4.2247	0.5180
ether	4.24	0.5192
chloroform	4.7113	0.5530
1-bromooctane	5.0244	0.5729
acetic acid	6.2528	0.6365
pentanal	10.0	0.75
dichloro ethane	10.125	0.7526
acetone	20.493	0.8666
ethanol	24.852	0.8883
methanol	32.613	0.9133
nitromethane	36.562	0.9222
dimethyl sulfoxide	46.826	0.9386
water	78.3553	0.9627
formamide	108.94	0.9730

Table 1 Solvents studied in this work, their permittivities ε and the corresponding *cmf* values. The values for ε were taken from the web page on the properties of the SCRF module of Gaussian Inc.

aug-cc-pVQZ] for the analysis of the effect of the basis set on the reaction barrier (Section S.1). The M05 calculated barrier of reaction 5 converges at approximately 110 kJ mol^{-1}. The M05/cc-VDZ method which worked very well for the properties of $(CH_3)_2S$ yields the lowest barrier of 84 kJ mol^{-1}. However, M05/6-311+G(2d,p) calculations obtain a barrier height of 110 kJ mol^{-1} which compares well with 110 kJ mol^{-1} obtained with the aug-cc-pVTZ basis set (σ_{tot} = 0.1243). Hence, the M05 functional with the 6-311+G(2d,p) basis set (σ_{tot} = 0.0815) was chosen to analyse the target reaction, the conversion of $(CH_3)_3SCl$.

The movement of the methyl group in reaction 1 is accompanied by a large charge transfer as the ionic charges quenched in this process. Changes in the total electron density, $\Delta\rho$, were analysed and visualised with the Visual Molecular Dynamics (vmd) program package[29] which provides an interface to Gaussian cube files. Atomic charges can be used to link $\Delta\rho$ to changes in covalence and ionicity in the CH_3-Cl and $(CH_3)_3S^+\cdots Cl^-$ bonds. Changes in APT[30,31] and NBO[32–35] charges provide a direct measure for the charge transfer from the Cl^- ion to the moving methyl group and formation of the covalent C−Cl bond.

Solvent effects were included into the quantum calculations by a polarizable continuum model (PCM).[36,37] The cavity was build from the radii of the UFF force field scaled by 1.1 as defined in the Gaussian 09 program package.[27] PCM calculations spanning a wide range of different solvents with the same cavity scaling factor are problematic, because the cavities differ in size on polar and apolar solvents. The Gaussian 09 default scaling factor of 1.1 is known to give good results for small ions such as Cl^- in water,[38] but is less likely to yield good results for low-permittivity solvents such as cyclohexane. The most important solvents in this study, ethanol (ε = 25), methanol (ε = 33) and water (ε = 78), are polar and protic, and the effect of scaling is expected to be of lesser importance for these solvents. Molecular properties are usually not linearly correlated with the permittivity ε of the solvent, while they tend to scale well with the Clausius-Mossotti factor (*cmf*)[39] of the solvent

$$cmf = \frac{\varepsilon - 1}{\varepsilon + 2} \quad . \tag{6}$$

This study includes 23 common solvents listed in Table 1. They were chosen either to match experimental conditions or to span the range of *cmf* values evenly. The energy of uncharged molecules such as CH_3Cl and $(CH_3)_2S$ is a linear function of the *cmf* while that of charged species [herein $(CH_3)_3S^+$, Cl^-, CH_3^+] shows a small deviation. The nonlinear data were fitted with two independent lines; the first group contains points up to ether (*cmf* = 0.52) and the second set starts from ether and up. Ether was chosen as the demarcation point, because it is the solvent with the lowest *cmf* value which supports a linear ion pair and its *cmf* value of 0.52 rests near the center of the *cmf* scale.

PCM geometry optimisations tend to converge less well than those for the vacuum. Smooth convergence was achieved with the RFO algorithm along with calculations of the force constants at each step. Additionally, the automatic trust-update was turned off, step size scaling enforced, and the maximum step size limited to 0.05 Bohr or radians. The harmonic force constants were calculated to confirm the identity of the stationary points and the unscaled harmonic frequencies were used to estimate changes in Gibbs free energy at 298.15 K and 1 atm. Reaction paths on the PES of the conversion reaction were established with the constrained reduced dimensionality (CRD) algorithm.[40] All minimum energy structures show no imaginary frequency and all transition state structures have one and only one imaginary frequency (Section S.3). All energies stated in this paper are reported relative to $(CH_3)_3S^+_{(sol)}$ and $Cl^-_{(sol)}$ infinitely separated from each other in the same chemical environment.

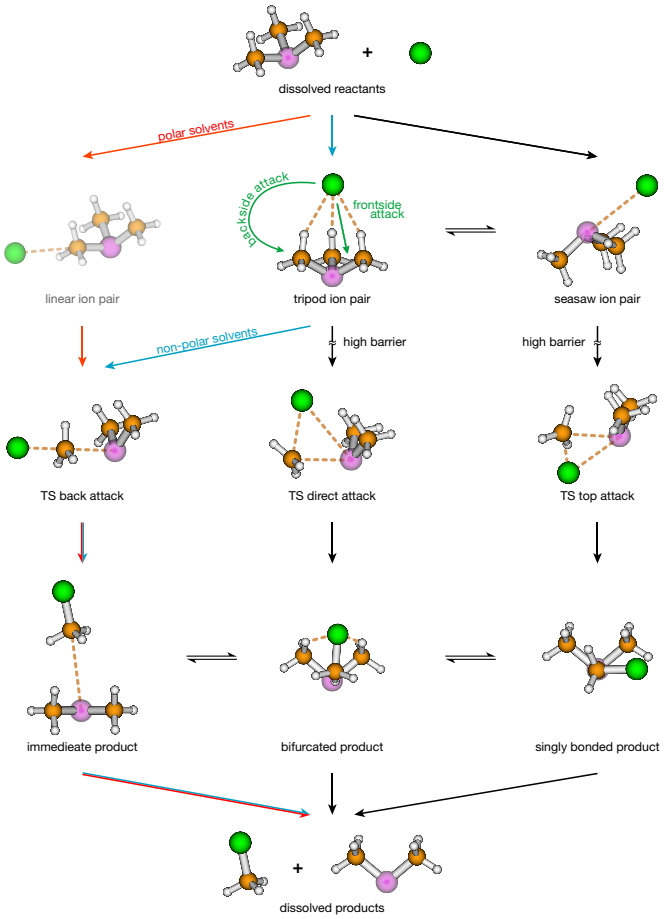

Scheme 1 Key structures on the potential energy surface of reaction 1 using Molden[43]. The linear ion pair is not a stationary point (Section 3.3.2) and is greyed to distinguish it from the calculated stationary points; however, the reaction path from the ions $(CH_3)_3S^+$ and Cl^- at infinite separation dissolved in polar solvents to the transition state for a backside attack passes through this geometry. The dominating reaction path in polar solvents is marked in red and that in non-polar solvents in blue. The Cl atom is shown in green, S in purple, C in orange and H in grey/white.

Standard Gibbs free energy calculations assume a gaseous environment, but solvolysis reactions are usually done in condensed media.[41,42] One mole of an ideal gas has a volume 24.5 L at 1013 mbar and 25 °C. To reach a standard concentration of 1 mol/L, the particle concentration in the gas phase has to be increased 24.5 fold; hence with T = 25 °C and p = 1 atm ΔG for a reaction is corrected with the addition of ΔG defined as following

$$\delta G = \Delta\xi \; R\,T \; \ln\left(\frac{R\,T}{p\;(10^{-3}\;\mathrm{m}^3)}\right) = \Delta\xi \; 7.926\;\mathrm{kJ/mol} \qquad (7)$$

where $\Delta\xi = \sum\xi_{\mathrm{pro}} - \sum\xi_{\mathrm{reac}}$ is the total change in the stoechiometric factors ξ_i. Equation 7 is applied to transition states, intermediates and products whenever absolute values of Gibbs free energies are required or δG does not cancel from an equation.

3 Energies and Reaction Paths

3.1 Key Structures and Paths for S_N2 Reactions

Scheme 1 shows the structures of selected stationary points on the potential energy surface (PES) of $(CH_3)_3SCl$. Structural information of all stationary points are provided in the last section of the ESI. The highly symmetric tripod ion pair has been reported[25] to be the most stable ion pair configuration. The ion pair with a direct S···Cl interaction has a less symmetric seesaw structure. The linear ion pair has a structure as to be expected for the reactive complex in a S_N2 reaction.[24] The linear transition state is expected for a standard S_N2 reaction with a backside attack. The next one, called 'TS direct attack' is the transition state to be expected for an attack of the chloride ion directly from its position in the tripod ion pair as opposed to the transition for a 'top attack' in which the chloride ion in a seesaw ion pair is inserted into the C−S bond.

The other three structures depict possible product clusters. The bifurcated product cluster with one CH···S and two Cl···HC bonds can be formed readily from the immediate product. The product cluster with a single CH···S bond is formed from the bifurcated product by a rotation of the CH_3Cl molecule.

3.2 Vacuum

Three minimum energy structures have been located on the PES of $(CH_3)_3S^+\cdot Cl^-$ for the reaction *in vacuo*: the tripod ion pair (ΔE_{tri} = −425 kJ mol^{-1}, ΔG_{tri} = −393 kJ mol^{-1}), the seesaw ion pair (ΔE_{see} = −411 kJ mol^{-1}, ΔG_{see} = −379 kJ mol^{-1}) and the immediate product cluster (ΔE_{pro} = −492 kJ mol^{-1}, ΔG_{pro} = −474 kJ mol^{-1}). The transition state ($\Delta E^{\ddagger}$ = −336 kJ mol^{-1}, $\Delta G^{\ddagger}$ = −313 kJ mol^{-1}) linking the tripod ion pair with the product cluster has a linear structure, but no stable linear ion pair as a reactive complex was found on the vacuum PES. The dissociation of the product cluster reduces the Gibbs free energy of the reaction even further (ΔE_{reac} = −485 kJ mol^{-1}, ΔG_{reac} = −504 kJ mol^{-1}). The energy of the backside transition state is much lower than that of the ions $(CH_3)_3S^+$ and Cl^- at infinite separation.

The $[(CH_3)_3S^+\cdot I^-]^{\mathrm{tri}}_{(\mathrm{vac})}$ tripod ion pair has been reported as the most stable ion pair in the vacuum.[25] The APT[30,31] and NBO[32–35] charge analysis of $[(CH_3)_3S^+\cdot Cl^-]^{\mathrm{tri}}_{(\mathrm{vac})}$ singles out the sulfur atom as the carrier of the largest positive charge (APT: 0.338 e, NBO: 0.770 e) while the bonding hydrogen atoms carry a significantly smaller charge (APT: 0.202 e, NBO 0.311 e). Nevertheless, the three hydrogen atoms together

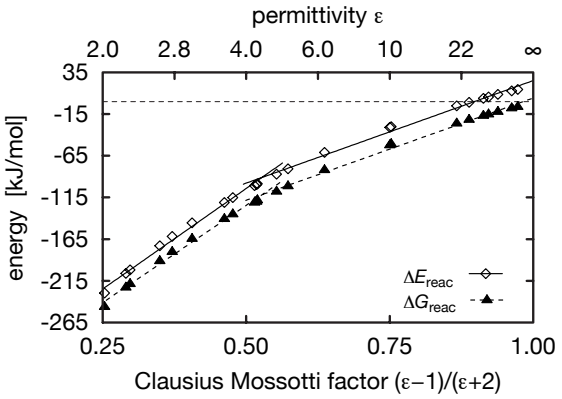

Fig. 1 Energies of formation of $CH_3Cl_{(sol)}$ and $(CH_3)_2S_{(sol)}$ from the free ions $(CH_3)_3S^+_{(sol)}$ and $Cl^-_{(sol)}$ at infinite separation.

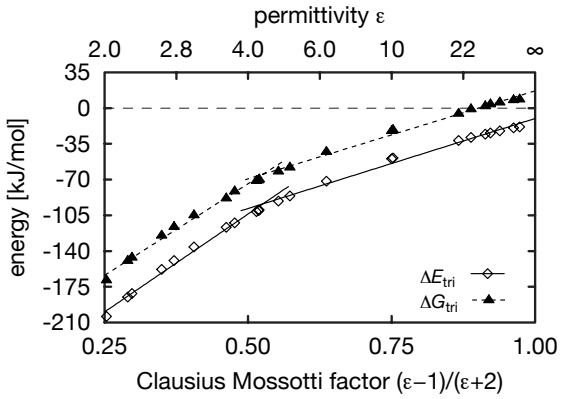

Fig. 2 Energies of formation of the ion pair with tripod geometry relative to the energy of the ions $(CH_3)_3S^+$ and Cl^- at infinite separation without particle density correction.

form a greater attractor for the chloride ion (APT: −0.896 e, NBO: −0.761 e) than the sulfur atom alone. A similar effect can be observed in the crystal structure[44] of $(CH_3)_3SI$ where the iodide ion is surrounded by hydrogen atoms from methyl groups.

The M05/6-311+G(2d,p) calculations yield −485 kJ mol^{-1} for ΔE_{reac} and the inclusion of the zero point energies ΔE^{ZP}_{reac} results in −490 kJ mol^{-1} while the calculation of the enthalpies at 298.15 K yields a value of −490 kJ mol^{-1} for ΔH_{reac} compared with −467 kJ mol^{-1} calculated from experimental data.[24]

3.3 S_N2 Reactions in Solultion

3.3.1 Overall Energy Changes. Figure 1 shows the reaction energies ΔE_{reac} and ΔG_{reac} as a function of *cmf* (Equation 6). The data are fitted with two straight lines. The general increase of ΔG_{reac} in Figure 1 indicates a continuous increase of the sulfonium salt represented by its ions (Equation 1) in the reaction mixture as the *cmf* value increases. A similar effect of the formation of $(CH_3)_3SI$ in various solvents has been reported[45] as the yield of the salt increases with the permittivity of the solvent. The DFT calculations predict reaction 1 to become endotherm going from *cmf* = 0.89 (ethanol) to *cmf* = 0.91 (methanol) whereas the Gibbs free energy of reaction 1 is estimated to be exergonic in all solvents due to the dissociation of the product cluster. The data for water (ΔG_{reac} = −8 kJ mol^{-1}, $K_{H_2O} \approx 25$) suggest that about 9 mole % of the reaction mixture is the salt.

3.3.2 Ion Pairs. A stable tripod ion pair $[(CH_3)_3S^+ \cdot Cl^-]^{tri}_{(sol)}$ can be found in all solvents. Coulomb interaction between the ions dominate the energy of formation ΔE_{tri} of the tripod ion pair. The weakness of the $Cl^- \cdots H$ interactions is reflected in the lack of charge transfer in the ion pair (Section S.2, Figure S.3). The APT charge on the chloride ion (cyclohexane: −0.97 *e*, formamide: −1.05 *e*) saturates quickly while the charge on the sulfur atom becomes more positive as the permittivity of the solvent increases. Figure 2 summarises the influence of the solvent on the energy of the tripod ion pair (ΔE_{tri} and ΔG_{tri}). The formation of the tripod ion pair is exotherm, but becomes endergonic at a *cmf* value of 0.90 ± 0.03 (ε = 28.5 ± 1.1). The correction of ΔG_{tri} for the different particle densities in the gas phase and solution (Equation 7) predicts ΔG_{tri} to become zero in solvents with a much higher permittivity of 55.2 ± 1.1.

Conductivity experiments with dimethyl-*t*butyl sulfonium salts[17,21] indicate that ion pairs are formed in solvents with a permittivity smaller than 25 which generally agrees with experiments using tribenzyl sulfonium chloride[13] suggesting that no ion pairs are formed in 90% (by volume) acetone (ε = 26.3,[46] ε = 25.3,[47] ε = 21 ± 5[48]). These experimental values are close to the value of 28.5 ± 1.1 calculated from the uncorrected values of ΔG_{tri}. On the other hand, reported values for the association constant K_A (Equation 3) of trimethylsulfonium iodide (6.6 L/mol[21]), dimethyl-*t*butyl sulfonium iodide (∼20 L/mol[18]) and dimethyl-*t*butyl sulfonium chloride (∼100 L/mol[18]) indicate significant ion pair concentrations even in pure water. The particle density corrected (Equation 7) value for ΔG_{tri} being 0.13 kJ mol^{-1} is in reasonably good agreement with a value of −4.7 kJ mol^{-1} calculated from the association constant K_A of $(CH_3)_3SI$, where a higher degree of association is expected due to the lower enthalpy of hydration of the I^- ion.

Selected properties of the seesaw ion pair in different media are listed in Table 2. The Gibbs free energy of the seesaw ion pair increases as the environment becomes more polar and ΔG_{see} is always higher than the Gibbs free energy of the tripod ion pair. However, the energy difference between the ion pairs becomes smaller as the permittivity of the solvent increases. The approximate equilibrium constant of 0.39 in water sug-

	vacuum	ether	water
ΔG_{see}	−379.309	−63.154	10.413
$\Delta^{tri}_{see}G$	13.792	6.543	2.355
$r_{S\cdots Cl}$	288.6	346.1	372.2
WBI S···Cl	0.1215	0.0132	0.0042
WBI S−C_{ax}	0.9401	1.0045	1.0079
WBI S−C_{eq}	1.0048	1.0092	1.0081
q^{NBO}_{Cl}	−0.8571	−0.9630	−0.9802
q^{APT}_{Cl}	−0.9492	−1.0256	−1.0434
μ	10.8020	16.2363	18.4160

Table 2 Properties of the seesaw ion pair in selected environments. ΔG_{see}: ΔG in kJ/mol relative to the ions $(CH_3)_3S^+$ and Cl^- at infinite separation, $\Delta^{tri}_{see}G$: ΔG in kJ/mol relative to the tripod ion pair, r: bond length in pm, WBI: Wiberg bond index, C_{ax}: axial carbon atom, C_{eq}: equatorial carbon atom, q^{NBO}: NBO charge in e, q^{APT}: APT charge in e, μ: dipole moment in Debye.

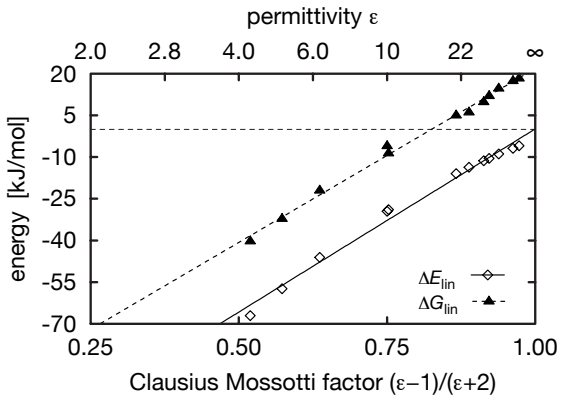

Fig. 3 Energies of formation of the linear reactive complex relative to the energy of the ions $(CH_3)_3S^+$ and Cl^- at infinite separation without particle density correction.

gests a 2:5 ratio between the two pairs. In combination with the data in Figure 2 the small difference $\Delta^{tri}_{see}G$ for the tripod and seesaw ion pair suggests that both ion pairs might simultaneously exist in a solution of $[(CH_3)_3SI]$ in D_2O where ^{33}S NMR spectra were not able to distinguish between paired and free ions.[25]

The structure of the seesaw ion pair suggests a partially covalent character of the S···Cl bond. The data in Table 2 seem to confirm this assumption with the comparatively short bond length and a Wiberg index of 0.12 for the S···Cl bond. The Wiberg indices for the C−S bonds also reveal different bond strengths between axial and equatorial carbon and sulfur atoms as observed in SCl_4, though to a lesser extent. In condensed media, the difference between the S−C bonds vanishes quickly and the electronic structure of the $(CH_3)_3S^+$ ion

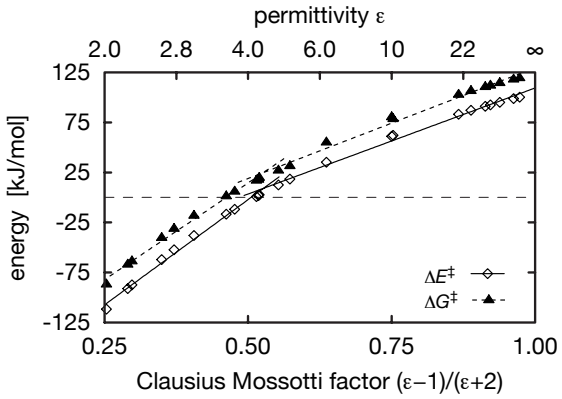

Fig. 4 Energies of formation of the linear transition state relative to the energy of the ions $(CH_3)_3S^+$ and Cl^- at infinite separation without particle density correction.

resembles that of a free $(CH_3)_3S^+$ ion as the S···Cl bond length increases. Furthermore, the NBO bond analysis does not support a bonding S···Cl orbital and the high charges on chloride ion also indicate an ionic bond. Hence, the structure of the seesaw ion pair seems to be the result of the repulsion between the Cl^- ion and the lone pair electrons on the sulfur atom.

Figure 3 shows the energy of the linear pair $[(CH_3)_3S^+\cdot Cl^-]^{lin}_{(sol)}$ as a function of the solvent's *cmf*. A linear minimum can only be found in calculations with a permittivity larger than or equal to 4.24 (ether). Its formation is exotherm; however, becomes endergonic at a *cmf* value of 0.83 ± 0.03 ($\varepsilon = 15.2 \pm 3.2$). This result agrees with other computational data[24] reporting linear ion pairs in ethanol (*cmf* = 0.89) and water (*cmf* = 0.96), but not for the vacuum. However, the careful examination of the very small barrier of 0.2 kJ mol^{-1} separating the tripod ion pair from the linear one in water suggests that the linear ion pair as a stationary point is a computational artefact.

3.3.3 Transition States. The linear transition state can be accessed either directly from free ions or from the tripod ion pair as shown in Scheme 1. Figure 4 shows its energy relative to that of the ions $(CH_3)_3S^+$ and Cl^- at infinite separation a function of the *cmf*. The energy of the transition state $\Delta E^‡$ of reaction 1 is lower than that of the $(CH_3)_3S^+$ and Cl^- in solvents with a *cmf* smaller than 0.51 (ethyl phenyl ether, $\varepsilon = 4.18$) and $\Delta G^‡$ is smaller than the Gibbs free energy of $(CH_3)_3S^+$ and Cl^- in solvents with a *cmf* smaller than 0.46 (diethyl amine, $\varepsilon = 3.58$). HF calculations with different basis sets[24] yield values between 129.7 and 136 kJ mol^{-1} for $\Delta E^‡_{H_2O}$ whereas the M05/6-311+G(2d,p) calculations obtain a value of 99 kJ mol^{-1} for $\Delta E^‡_{H_2O}$ and a value of 118 kJ mol^{-1} for $\Delta G^‡_{H_2O}$ (corrected 110 kJ mol^{-1}).

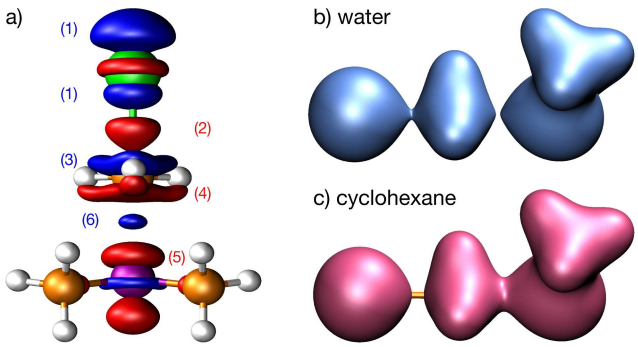

Fig. 5 Analysis of the electronic structure of the linear transition state in cyclohexane and in water. a) Isosurface of the difference of the electron densities $\Delta\rho$ in cyclohexane and water with a fixed geometry. Selected lobes are labeled with small arabic numbers. Atoms coloured the same as in Scheme 1. Red surface: +0.0012, blue surface: −0.0012. b) Isosurface ($\rho = 0.055$) of the total electron density in water (optimised geometry) c) Isosurface ($\rho = 0.055$) of the total electron density in cyclohexane (optimised geometry).

The energy of the transition state increases as the solvent becomes more polar (Figure 4). This result agrees with the observation that the rate of the solvolysis reaction is higher in ethanol than in water.[12,14,17] The Gibbs free energy of the bipolar transition state is 45 kJ mol^{-1} higher in cyclohexane than in formamide as expected from Coulombic interactions between solute and solvent. Meanwhile, the Gibbs free energy of the ions $(CH_3)_3S^+$ and Cl^- is 251 kJ mol^{-1} higher in C_6H_{12} than in $HCONH_2$ which results in the increase of $\Delta G^{\ddagger}$ by 206 kJ mol^{-1}.

Figure 5.a shows the difference ($\Delta\rho = \rho_{C_6H_{12}} - \rho_{H_2O}$) between the total electron density ρ of the transition state in cyclohexane (C_6H_{12}) and water. The density calculations were done using the ether geometry, because the S-Cl distance in the ether geometry (467 pm) is close to the average (466 pm) of the cyclohexane (463 pm) and water (470 pm) geometries. Negative values indicate regions with an increased electron density in water whereas positive values show regions with an increased electron density in cyclohexane. Water as a solvent stabilises the negative charge on the chloride ion as indicated by the big, blue lobes labeled as (1) in Figure 5.a. The lack of stabilisation in cyclohexane leads to an increase in electron density along the C···Cl bond (2). However, this electron density is likely to be found close to methyl group (3) in water. The lobes (4) and (5) show that the electron density is closer to the CH_3 and $(CH_3)_2S$ units in cyclohexane than in water. The small negative lobe (6) suggests that the reduction of the polarisation by the Cl^- ion leads to a small increase of electron density along the S···C bond.

Figures 5.b and 5.c show the isosurfaces of the total electron density in water and cyclohexane using the optimised geometries for the density calculations. The S···C bond is longer in water (239 pm) than in cyclohexane (226 pm). This increase in bond length is likely to cancel the increase in electron density as indicated in lobe (6). The C···Cl bond is shorter in water (231 pm) than in cyclohexane (238 pm), but the shorter bond length is not accompanied by a sizeable increase of electron density along the C···Cl bond which suggests that the ionic character of the C···Cl bond is maintained both in cyclohexane and in water.

	vacuum		water	
bond	Cl−C	C−S	Cl−C	C−S
transition state	0.3909	0.6134	0.4780	0.4627
CH_3Cl	1.0373	—	1.0226	—
$(CH_3)_3S^+$	—	1.0079	—	1.0086
$(CH_3)_2S$	—	1.0402	—	1.0381

Table 3 Selected Wiberg bond indices during a backside attack.

The Wiberg bond index[51,52] of the C···S bond decreases from 0.61 in vacuum to 0.46 in water while the bond index of the Cl···C bond increases from 0.39 to 0.48 (Table 3). The comparison with the bond indices in CH_3Cl, $(CH_3)_2S$ and $(CH_3)_3S^+$ in Table 3 suggests that the C···Cl bond is half-formed and the C···S bond is half-broken in the transition state. On the other hand, the NBO analysis does not find a bonding orbital between Cl^- and the moving CH_3 group in agreement with the analysis of the canonical orbitals and that of the elctron densities. The Cl···C bond in the transition state is dominated by Coulomb interactions while covalent interactions dominate the C···S bond.

The CH_3 group moves closer to the Cl^- ion while the C···S bond becomes weaker as the *cmf* value of the solvent increases. The transition state in solvents with a high permittivity resembles thereby more the products CH_3Cl and $(CH_3)_2S$ than it resembles the reactants $(CH_3)_3S^+$ and Cl^- while reaction 1 becomes increasingly more endothermic (Figure 1) which would classify it as a late transition state according to the Hammond postulate[49,50] in contrast to an early one in apolar solvents. The lateness of these transition states can be observed in the depolarisation of the $(CH_3)_2S$ subunit. The NBO charge[32–35] on the $(CH_3)_2S$ subunit decreases from 0.528 *e* in the vacuum to 0.380 *e* in water. One third of the necessary negative charge formally originates from the Cl^- ion and the rest from the moving methyl group whose charge increased by only 0.1 *e* from vacuum to water.

Table 4 sumarizes selected properties of the transition states for frontside attacks in different environments starting from either the tripod (direct TS) or the seesaw ion pair (top TS) as shown in Scheme 1. The calculations for an attack starting from the seesaw ion pair were done with the assumption that the chloride ion attacks the neighbouring methyl group in the equatorial position. This attacking path is largely

	vacuum		ether		water	
	direct TS	top TS	direct TS	top TS	direct TS	top TS
$\Delta G^{\ddagger}_{\text{front}}$	−221.910	−214.839	140.908	143.620	238.957	235.523
$\Delta^{\text{back}}_{\text{front}} E^{\ddagger}$	95.905	101.092	123.455	122.539	127.628	122.968
$\Delta^{\text{back}}_{\text{front}} G^{\ddagger}$	90.863	97.934	121.178	123.889	121.038	117.604
$r_{\text{C}\cdots\text{S}}$	267.8	250.6	271.5	260.4	275.1	267.4
$r_{\text{Cl}\cdots\text{C}}$	262.2	252.2	268.1	260.9	270.4	262.9
WBI C···S	0.4153	0.4565	0.4094	0.4356	0.3979	0.4091
WBI Cl···C	0.4414	0.4565	0.3809	0.3958	0.3508	0.3721
$q^{\text{NBO}}_{\text{CH}_3}$	0.333	0.264	0.418	0.371	0.464	0.430
$\Delta^{\text{back}}_{\text{front}} q^{\text{NBO}}_{\text{CH}_3}$	+0.193	+0.123	+0.203	+0.156	+0.224	+0.190

Table 4 Properties of the transition states for a frontside attacks as shown in Scheme 1. WBI: Wiberg bond index, $q^{\text{NBO}}_{\text{CH}_3}$: NBO charge on the moving CH_3 group in multiples of *e*. All energies in kJ/mol, and all distances in pm. Transition state searches for the front site transition state were done with an ultra fine grid and all transition states have only one imaginary frequency. The energies are extrapolated to those to be expected from calculations with a standard grid for comparison.

controlled by the steric interactions between the chloride ion and the hydrogen atoms of the methyl groups, which forces the Cl^- ion on a curved path out of the symmetry plane of the $(CH_3)_2S\cdots CH_3^+$ subunit. The general arrangement of the methyl-hydrogen atoms of the ion pair is conserved in the direct transition states in water and ether (Scheme 1) while the moving methyl group is rotated by 60° around its c_3 axis in the transition state in the vacuum.

The Gibbs free energy $\Delta G^{\ddagger}_{\text{front}}$ of the transition states increases with the permittivity of the solvent similarly to the linear transition state. The ionic character of moving methyl group increases with the permitivity of the solvent and a comparison with the Wiberg indices for a backside attack (Table 3) shows that the moving methyl group is less tightly bound during a frontside attack. More importantly, the Gibbs free energy of the transitions states for a frontside attack is about 100 kJ mol^{-1} higher than that for a backside attack (Table 4); hence, a frontside reaction exploiting the proximity of the ions in the ion pairs is likely to play only a minor role if not none in the conversion of $(CH_3)_3SCl$.

3.3.4 Product Cluster. The energies of formation ΔE_{pro} and ΔG_{pro} (Figure 6) of the immediate product cluster (one C···S bond from back attack TS) show that its formation is endergonic in solvents with a *cmf* value of 0.87 (acetone) and endotherm at 0.92 (nitromethane). All three clusters, the immediate product cluster, the bifurcated one (two Cl···HC and one CH···S bond from the direct attack TS) and the singly bonded product cluster (one CH···S bond from the top attack TS) have nearly the same Gibbs free energy of formation in water (22, 21, and 22 kJ mol^{-1}; in the given order) as to be expected for the weak interactions between CH_3Cl and $(CH_3)_2S$. However, none of these product clusters is stable against dissociation. For example, ΔG_{diss} for the dissociation of the immediate product cluster is −30 kJ mol^{-1} in water. Hence, the product clusters are not likely to play a major role on the exit channel of the conversion reaction and the solvated CH_3Cl and $(CH_3)_2S$ molecules are the final products of the reaction.

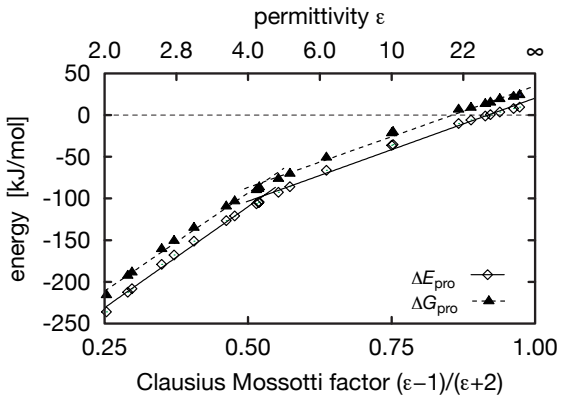

Fig. 6 Energy of formation of the immediate product complex relative to the energy of the ions $(CH_3)_3S^+$ and Cl^- at infinite separation without particle density correction.

3.4 Reactions involving CH_3^+ ions.

An extreme version of the dissociation of the carbon-sulfur bond is the classic S_N1 reaction

$$(CH_3)_3S^+_{(sol)} \xrightarrow{k_{S_N1}} (CH_3)_2S_{(sol)} + CH^+_{3(sol)} \quad (8)$$

$$CH^+_{3(sol)} + Cl^-_{(sol)} \longrightarrow CH_3Cl_{(sol)} \quad . \quad (9)$$

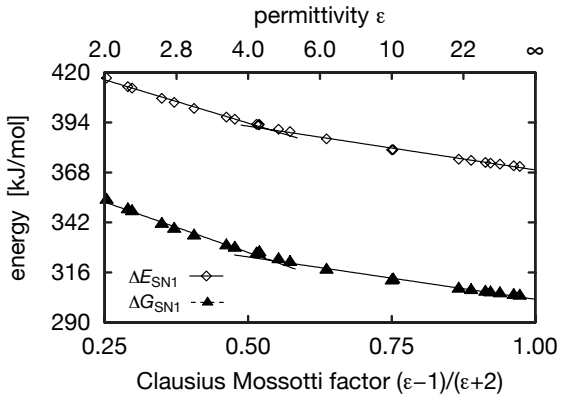

Fig. 7 Combined energy of $(CH_3)_2S$, CH_3^+ and Cl^- relative to the ions $(CH_3)_3S^+$ and Cl^- at infinite separation without particle density correction.

The small methyl cation is unlikely to form,[53] but it is worth to explore carefully the possibilities of its formation in extremely polar solvents to complete the analysis of the reaction mechanism. The combined energies (ΔE_{S_N1} and ΔG_{S_N1}) of CH_3^+, $(CH_3)_2S$ and Cl^- relative to the energies of $(CH_3)_3S^+$ and Cl^- at infinite separation decrease rapidly as the permittivity of the solvent increases (Figure 7). The comparison with Figure 4 shows that ΔG_{S_N1} is always significantly larger than $\Delta G^{\ddagger}$; even if the permittivity ε of the solvent becomes infinite ($cmf = 1$). Consequently, any mechanism based on the formation of a free methyl cation can be ruled out for the conversion of trimethylsulfonium chloride.

A less dramatic version of the reaction might proceed *via* an ion-dipole assemblage[54]

$$(CH_3)_3S^+_{(sol)} \longrightarrow [(CH_3)_2S{\cdot}CH_3^+]_{(sol)} \tag{10}$$

$$[(CH_3)_2S{\cdot}CH_3^+]_{(sol)} + Cl^-_{(sol)} \longrightarrow (CH_3)_2S_{(sol)} + CH_3Cl_{(sol)}\ , \tag{11}$$

but a scan of the relaxed potential energy surface of the dissociation for the S−C bond of the $(CH_3)_3S^+$ ion in water gives no indication for such an ion-dipole assemblage so that this pathway has to be ruled out for the conversion of $(CH_3)_3SCl$, too. In summary, mechanisms involving the formation of CH_3^+ are unlikely to contribute to reaction 1.

3.5 Hydrolysis

Since water is generally more reactive than methanol or ethanol, the hydrolysis of $(CH_3)_3SCl_{(aq)}$

$$(CH_3)_3S^+_{(aq)} + Cl^-_{(aq)} + H_2O_{(aq)} \longrightarrow (CH_3)_2S_{(aq)} + CH_3OH_{(aq)} + H^+_{(aq)} + Cl^-_{(aq)} \tag{12}$$

was chosen as an example to analyse the competition between solvolysis and the conversion according to Equation 1. The dissociation of $(CH_3)_3S^+_{(aq)}$ yields a CH_3^+ cation (Equation 8) which initiates the formation of CH_3OH

$$CH^+_{3(aq)} + H_2O_{(aq)} \longrightarrow CH_3OH^+_{2(aq)} \longrightarrow CH_3OH_{(aq)} + H^+_{(aq)}\ . \tag{13}$$

Scans of the $CH_3^+{\cdot}H_2O$ potential energy surface along the C−O coordinate show that the formation of $CH_3OH_2^+$ is barrier-free in water, but the discussion in the preceeding section suggests that any reaction pathway involving free CH_3^+ ions is very unlikely to contribute to the overall reactivity of the system.

An alternative route of hydrolysis proceeds *via* a S_N2 type mechanism starting from the $(CH_3)_3S^+$ cation and water

$$H_2O_{(aq)} + (CH_3)_3S^+_{(aq)} \xrightarrow{k_{14}} (CH_3)_2S_{(aq)} + CH_3OH^+_{2(aq)} \tag{14}$$

$$CH_3OH^+_{2(aq)} \longrightarrow CH_3OH_{(aq)} + H^+_{(aq)}\ . \tag{15}$$

The un-corrected Gibbs free energy of the transition state in a S_N2 type hydrolysis (reaction 14) relative to H_2O and $(CH_3)_3S^+$ infinitely separated from each other ($\Delta_{14}E^{\ddagger}$ = 150 kJ mol^{-1}, $\Delta_{14}G^{\ddagger}$ = 189 kJ mol^{-1}, where the numerical subscript to the delta symbol indicates the numbered reaction for which the difference is defined. A list of all symbols is provided in Section S.3.) is much larger than the corresponding barrier for conversion reaction in water ($\Delta E^{\ddagger}_{H_2O}$ = 99 kJ mol^{-1}, $\Delta G^{\ddagger}_{H_2O}$ = 118 kJ mol^{-1}). This solvolysis pathway is kinetically less favourable than the conversion.

The calculation of $\Delta_{12}G$ for the solvation reaction was done in two steps to avoid PCM calculations with a single proton.[41,55]

$$(CH_3)_3S^+_{(aq)} + Cl^-_{(aq)} + H_2O_{(aq)} \longrightarrow (CH_3)_2S_{(aq)} + CH_3OH_{(aq)} + HCl_{(aq)} \tag{16}$$

$$HCl_{(aq)} \longrightarrow H^+_{(aq)} + Cl^-_{(aq)} \tag{17}$$

The Gibbs free energy change $\Delta_{12}G$ for the hydrolysis is equal to the sum of $\Delta_{16}G$ and $\Delta_{17}G$ which is calculated from the pK_A value of hydrochloric acid in water

$$\Delta_{17}G = \ln(10)\, R\, T\, pK_A \quad . \tag{18}$$

The pK_A of HCl in water was taken to be equal to −8.0 according to a table for acids compiled by Ripin and Evans[56] which yields a value of −46 kJ mol^{-1} for $\Delta_{17}G$ at 298.15 K. The hydrolysis is more exergonic ($\Delta_{12}G$ = −17 kJ mol^{-1}) than the conversion reaction (ΔG_{reac} = −8 kJ mol^{-1}).

Finally, macroscopic hydrolysis could originate from the conversion of the newly formed methyl chloride

$$CH_3Cl_{(aq)} + H_2O_{(aq)} \xrightarrow{k_{19}} CH_3OH^+_{2(aq)} + Cl^-_{(aq)} \quad (19)$$

$$CH_3OH^+_{2(aq)} \longrightarrow CH_3OH_{(aq)} + H^+_{(aq)} \, . \quad (20)$$

The uncorrected energies ($\Delta_{19}E^{\ddagger}$ = 129 kJ mol^{-1}, $\Delta_{19}G^{\ddagger}$ = 171 kJ mol^{-1}) for the hydrolysis of methyl chloride were found to be smaller than those for reaction 14, but still significantly larger than those for the conversion reaction. Looking at all three possibilities, hydrolysis does not appear to compete with the conversion since the barriers are significantly higher.

The data for the hydrolysis of CH_3Cl can be used for an independent evaluation of the computational method. The correction of $\Delta_{19}G^{\ddagger}$ for the particle concentrations (Equation 7, $\Delta\xi = -1$) yields a barrier height of 163 kJ mol^{-1} (39 kcal mol^{-1}) which compares reasonably well with the values of 28 kcal mol^{-1} (298 K) for $\Delta G^{\ddagger}$ and 28 kcal mol^{-1} (308 K) for energy of activation obtained from experiments.[57,58] Published quantum chemical calculations[59,60] for $\Delta_{19}E^{\ddagger}$ vary between 8 and 38 kcal mol^{-1} compared to 27 kcal mol^{-1} from experiments[58] and $\Delta_{19}H^{\ddagger}$ = 32 kcal mol^{-1} ($\Delta_{19}E^{\ddagger}$ = 31 kcal mol^{-1}) from the PCM calculations of the current study. Tabulated thermodynamical data[58,61] can be used to estimate the change in Gibbs free energy $\Delta_{19}G + \Delta_{20}G$ for the hydrolysis of CH_3Cl to be −12 kJ mol^{-1} which compares favourably to −9 kJ mol^{-1} obtained from our PCM calculations using a thermodynamic cycle similar to that shown in Equations 16 and 17.

The kinetic control of the solvolysis reaction has been reported by Pocker and Parker[62] in their study of $(CH_3)_3S^+X^-$ with X^- being a halide or pseudohalide. The hydrolysis of the sulfonium salt (reaction 12) can be detected by the formation of acid. No acid was detected in the first 30% of reaction 1. The reaction was not followed any further, because the reverse reaction of 1 and the hydrolysis of CH_3X interfered with the kinetic analysis. The uncorrected transition state energies for reactions 14 (189 kJ mol^{-1}) and 19 (171 kJ mol^{-1}) further support Pocker's and Parker's assumption that the solvolysis products stem from CH_3X and not from the direct solvolysis of the $(CH_3)_3S^+$ ion.

3.6 Explicit solvent molecules

The most severe limitation of the PCM from the chemical view point is the lack of explicit solute-solvent interactions in the calculation. A series of preliminary embedded ONIOM molecular dynamics simulations of a ball with a constant volume of 9001 Å^3 of 296 water molecules with the $(CH_3)_3S^+$ and Cl^- ions in the centre was done to create a set of geometries suitable to estimate the influence of explicit solute-solvent interactions on reaction 1. The amber force field was used for the solvent and OLYP/6-31G(d,p) DFT calculations (σ_{tot} = 0.158) as compromise between speed and quality for the solute. Both methods were used as supplied with the Gaussian09 suite of programs.[27] The charges on the solute atoms were obtained from averring the results from charge generating MD simulations. In these calculations, each force calculation was preceded by the calculation of the ESP charges on the solute atoms at HF/6-31G(d,p) level in a solvent free environment (Details in Section S.4).

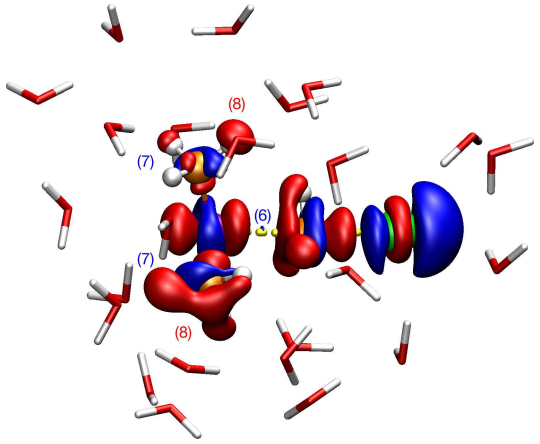

Fig. 8 Changes in the electronic density $\Delta\rho^{ex}$ of the linear transition state (fixed geometry) going from vacuum to liquid water (296 molecules). state in cyclohexane and in water. The 25 H_2O molecules of the first solvation shell are shown as liquorice. Cl: green, S: purple, O: red, C: orange, H: white, changing bond: dashed yellow bond, red surface: +0.0012, blue surface: −0.0012. The numberingg scheme of the lobes is continued from Figure 5.

The linear transition state was studied by freezing the S···C and C···Cl bond lengths at the values obtained from PCM calculation for water either with the M05/6-311+g(2d,p) [$r_{C\cdots S}$ = 239 pm, $r_{Cl\cdots C}$ = 231 pm] or with the OLYP/6-31G(d,p) setup [$r_{C\cdots S}$ = 237 pm, $r_{Cl\cdots C}$ = 237 pm]. The simulations with the M05/6-311+g(2d,p) bond lengths yielded a lower average of the total energy, and more importantly, smaller average gradients along the constrained bonds than the simulations with the OLYP/6-31G(d,p) bond lengths. Hence, the simulations with the more asymmetric set of bond lengths from the M05/6-311+g(2d,p) setup was used for the analysis.

The MD simulations at 298 K predict the transition state to be $\Delta U^{\ddagger}$ = 152 kJ mol^{-1} higher in inner energy and $\Delta H^{\ddagger}$ = 159 kJ mol^{-1} higher in enthalpy while the products are expected to be ΔU_{reac} = 75 kJ mol^{-1} higher in energy and ΔH_{reac} = 92 kJ mol^{-1} in enthalpy. The increase in enthalpy can be linked to an increase in pressure since the transition state and the products with their solvation shells need progressively more space as the reaction proceeds. The comparison with the OLYP-PCM calculations for water shows that the inclusion of explicit solute-solvent interactions into the calculations turned reaction 1 from slightly exothermic (OLYP/6-31G(d,p): ΔE_{reac} = −19 kJ mol^{-1}) to strongly exothermic

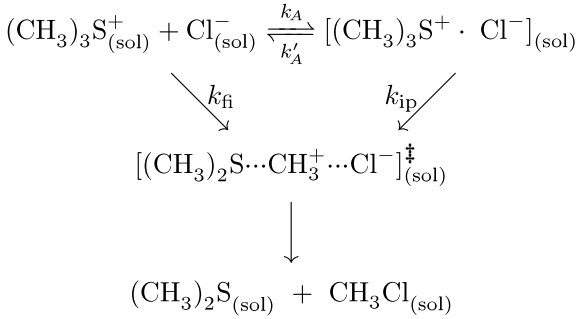

Scheme 2 Possible reaction pathways for the conversion of $(CH_3)_3SCl$. The free ions and the ion pair reaction pass through the same transition state $[(CH_3)_2S\cdots CH_3^+\cdots Cl^-]_{(sol)}$.

while raising the energy of the transition state (OLYP/6-31G(d,p): $\Delta E^{\ddagger}$ = 68 kJ mol^{-1}). This change can be traced back to the stabilisation of the chlorine atom in solution. The first solvation shell of the Cl^- ion comprises on average 7.2 water molecules which provide a stabilisation of -246 ± 22 kJ mol^{-1} while that of CH_3Cl contains on average 23.3 water molecules with a destabilising interaction energy of $+6 \pm 19$ kJ mol^{-1}.

Figure 8 shows the difference in the electron densities ($\Delta\rho^{ex} = \rho_{vac} - \rho^{ex}_{H_2O}$) between vacuum and water (296 molecules) with a fixed geometry. The shown cluster was chosen, because its potential energy matches that of the trajectory average. The colouring scheme and the isovalues are the same as in Figure 5 to simplify the comparison. Figures 8 and 5 show that the PCM fails to account for the influence of the water molecules onto the methyl groups in the $(CH_3)_3S^+$ ion (lobes 7 and 8). But, the lobes along the S···C···Cl [lobes (1) to (6)] axis are the same as in Figure 5, though larger in size with the exception of the small positive lobe (6) between the sulphur and the carbon atom. The very close similarity of the changes in electron density suggest that the PCM reproduces the chemically relevant changes in electron density for the transition state very well.

4 Kinetics

The mechanism for the conversion of $(CH_3)_3SCl$ is summarised in Scheme 2. The transition states for the frontside attacks and the solvolysis are so high in energy that these paths do not contribute to the overall reaction. The formation of CH_3^+ ions is energetically too costly so that S_N1-type reactions can be neglected, too. The three product clusters are unstable towards dissociation and they are not part of Scheme 2, either.

It is possible that the products are formed directly from the dissolved ions in solvents with a high permittivity. The free

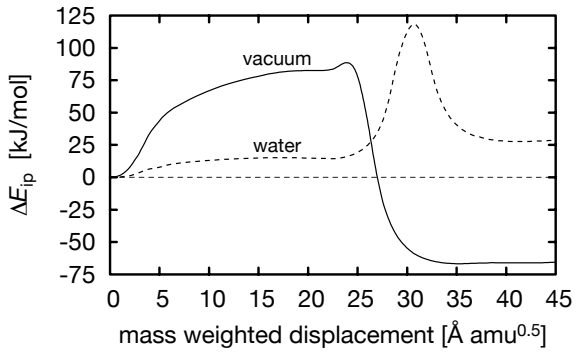

Fig. 9 Search for the path of the conversion reaction *in vacuo* and in water starting at the tripod ion pair passing through the linear transition state and ending at the immediate products. ΔE_{ip}: energy of the C_3H_9SCl cluster relative to that of the tripod ion pair. The data for the vacuum curve are taken from reference 40.

ions path proceeds *via* the linear transition state of a backside attack

$$(CH_3)_3S^+_{(sol)} + Cl^-_{(sol)} \xrightarrow{k_{fi}} (CH_3)_2S_{(sol)} + CH_3Cl_{(sol)} \quad . \tag{21}$$

The rate law is expected to be of first order in the concentration of each ion

$$v_{fi} = k_{fi}\,[(CH_3)_3S^+]\,[Cl^-]\;,\; k_{fi} = (k_B T/h)\; e^{-\Delta G^{\ddagger}/RT} \tag{22}$$

where k_{fi} is the free ions rate constant, $\Delta G^{\ddagger}$ is the difference in Gibbs free energy between the dissolved ions $(CH_3)_3S^+$ and Cl^- at infinite separation (free ions) G_{free} and the transition state $G^{\ddagger}$, and concentrations are indicated by square brackets. The natural limit of Equation 22 is given by $\Delta G^{\ddagger}$ equal to zero (ε = 3.58, *cmf* = 0.46).

Alternatively, the reaction can proceed *via* the tripod ion pair

$$(CH_3)_3S^+_{(sol)} + Cl^-_{(sol)} \underset{k'_A}{\overset{k_A}{\rightleftharpoons}} [(CH_3)_3S^+\cdot Cl^-]_{(sol)} \tag{23}$$

$$[(CH_3)_3S^+\cdot Cl^-]_{(sol)} \xrightarrow{k_{ip}} (CH_3)S_{(sol)} + CH_3Cl_{(sol)} \tag{24}$$

which becomes the reactant in solvents with a low permittivity. The CRD method[40] can be used to locate reaction paths starting from any point on the potential energy surface of the system, herein the tripod ion pair. The set of *predictors* used to span the reaction path was build from one S−C bond which increases in length during the search, one C···Cl bond which decreases in length and one S−C···Cl angle which increases in size to move the system through a linear backside transition state. The S−C···Cl angle was constrained to avoid cluster geometries with a S−C···Cl angle larger or equal to 180° during the search. An animation of the reaction path starting

at the linear transition state showing the link between the tripod ion pair, the linear transition state, the direct product and bifurcated product is provided as part of the supplementary material. The S−C···Cl angle increases rapidly in the initial phase of the search as the chloride ion moves into its attack position similar to that in the linear ion pair. At this point, the reaction path starting from the tripod ion pair joins that starting form the free ions. Then, correlated changes in the two bond lengths move a methyl group from its position in the $(CH_3)_3S^+$ cation into its final position in the methyl chloride molecule. The CRD reaction path starting at the tripod ion pair passes smoothly through the linear transition state and reveals no intermediate states (Figure 9). The smooth transition can be interpreted by the strong Coulomb interactions of the ion pair. The non-directional Coulomb forces are controlled solely by the distance between the charge centers of the ions and this distance changes smoothly along the reaction path. Solvents increase the mobility of the Cl^- ion in the ion pair as reflected in the heights of the plateaues for the Cl^- movement in the left hand side of Figure 9.

The rate of an ion pair mechanism is expected to be of first order in the ion pair concentration

$$v_{ip} = k_{ip}\,[(CH_3)_3S^+\cdot Cl^-]\;,\; k_{ip} = (k_B T/h)\; e^{-\Delta G^{\ddagger}_{ip}/RT} \qquad (25)$$

where $\Delta G^{\ddagger}_{ip}$ represents the difference in Gibbs free energy between the tripod ion pair G_{ip} and the linear transition state $G^{\ddagger}$.

The association constant K_A becomes very large in solvents with a low permittivity. In this case, the salt concentration becomes equal to the concentration of tripod ion pair and the rate v of the reaction becomes equal to

$$v = k_{ip}\,[(CH_3)_3SCl] \qquad (26)$$

where $[(CH_3)_3SCl]$ is the concentration of $(CH_3)_3SCl$.

In solvents with a medium permittivity, the free ions and the ion pair form an equilibrium and the simplification in Equation 26 is not valid anymore. The ion pair concentration $[(CH_3)_3S^+\cdot Cl^-]$ in Equation 25 can be obtained from the law of mass action for the equilibrium

$$[(CH_3)_3S^+\cdot Cl^-] = K_A\,[(CH_3)_3S^+]\,[Cl^-] \qquad (27)$$

where K_A is the association constant for formation of the tripod ion pair and hence concentration law for the ion pair reaction becomes

$$\begin{aligned} v_{ip} &= k_{ip}\,K_A\,[(CH_3)_3S^+]\,[Cl^-] \\ &= k_{28}\,[(CH_3)_3S^+]\,[Cl^-] \quad . \end{aligned} \qquad (28)$$

The combined rates for the reaction starting either from ion pairs or the free ions is given by

$$\begin{aligned} v = v_{fi} + v_{ip} &= (k_{fi} + k_{ip}\,K_A)\,[(CH_3)_3S^+]\,[Cl^-] \\ &= k_{29}\,[(CH_3)_3S^+]\,[Cl^-] \quad . \end{aligned} \qquad (29)$$

solvent	T	χ_{fi}	χ_{ip}	χ_{1mM}	χ_{10mM}
EtOH	373.15	38.50	2.144	38.44	37.91
EtOH	351.55	48.57	2.248	48.29	45.99
EtOH	298.15	99.88	2.622	88.49	45.37
Me_2CO	298.15	461.9	2.108	207.3	30.96
Et_2O	298.15	—	3801	4009	4007
C_6H_{12}	298.15	—	83937	88516	88477

Table 5 Acceleration factor χ (Equation 31) for ethanol (EtOH), acetone (Me_2CO), ether (Et_2O) and cyclohexane (C_6H_{12}) using water as reference. T: temperature in K, χ_{fi}: using $\Delta G^{\ddagger} = G^{\ddagger} - G_{free}$ (Equation 22), χ_{ip}: using $\Delta G^{\ddagger}_{ip} = G^{\ddagger} - G_{ip}$ (Equation 25), χ_{1mM}: using Equation 33 and $c_0 = 0.001$ Mol L^{-1}, χ_{10mM}: using Equation 33 and $c_0 = 0.01$ Mol L^{-1}.

Kinetic experiments can provide the lump constant k_{29}, but cannot distinguish between its components k_{fi}, k_{ip} and K_A.

Transition state theory yields the rate constant k_{28} of the reaction stating from ion pairs

$$k_{28} = k_{ip}\,K_A \propto \exp\left(\frac{-(\Delta G^{\ddagger}_{ip} + \Delta G_{ip})}{RT}\right) = \exp\left(\frac{-\Delta G^{\ddagger}}{RT}\right) \qquad (30)$$

since $\Delta G^{\ddagger}_{ip} = G^{\ddagger} - G_{ip}$ and $\Delta G_{ip} = G_{ip} - G_{free}$. The equation for the overall rate of ion pair mechanism is equal to that for free ions path (Equation 22) as both paths run through the same transition state. The two pathways are indistinguishable in solvents with an intermediate permittivity as discussed by Pocker and Parker for $(CH_3)_3SBr$.[62]

The kinetic solvent effect (KSE) of the solvolysis reaction (Equation 2) in solvents with an intermediate permittivity has been analysed previously[12,14,17] by using water and ethanol as solvents. If $\Delta G^{\ddagger}$ is larger than zero for both solvents, Equation 22 can be used to calculate the acceleration factor χ of the conversion reaction assuming similar values for the transmission coefficients in both solvents (Table 5).

$$\chi_{fi} = \frac{k_{fi}^{EtOH}}{k_{fi}^{H_2O}} \approx \exp\left(\frac{-\Delta G^{\ddagger}_{EtOH} + \Delta G^{\ddagger}_{H_2O}}{RT}\right) \quad . \qquad (31)$$

An alternative analysis starts from Equation 25. Since the tripod ion pair can be observed in all solvents, it is assumed that the conversion reaction runs exclusively *via* the tripod ion pair exploiting the vicinity of the reacting ions. Furthermore, the reaction is limited by the small values of K_A in polar solvents. In water, for example, the association constant K_A for the formation of ion pairs is 0.95 at 25 °C with the correction for particle densities (Equation 7). In this ion pair based scenario, the barrier is equal to $\Delta G^{\ddagger}_{ip}$. The results of the acceleration obtained with Equation 31 using $\Delta G^{\ddagger}_{ip}$ instead of $\Delta G^{\ddagger}$

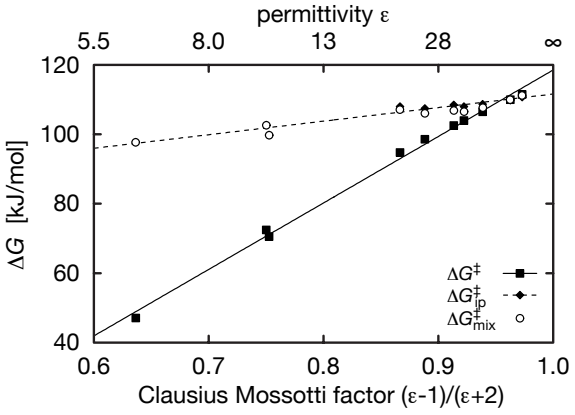

Fig. 10 $\Delta G^{\ddagger}$, $\Delta G^{\ddagger}_{\mathrm{ip}}$ and $\Delta G^{\ddagger}_{\mathrm{mix}}$ for c_0 = 1 M corrected for δG as a function of *cmf*.

are listed in Table 5, too. The solvent dependence of $\Delta G^{\ddagger}_{\mathrm{ip}}$ is much smaller than that of $\Delta G^{\ddagger}$, because the Gibbs free energy of the tripod ion pair changes by only 74 kJ mol^{-1} compared to 251 kJ mol^{-1} for the dissolved ions $(CH_3)_3S^+$ and Cl^- at infinite separation in cyclohexane and formamide.

The computational model does not contain thermal fluctuations of the solvent. It is therefore impossible to estimate the dynamics of the equilibrium between the free ions and the ion pairs, how the viscosity of the solvent affects the speed of formation of the linear transition state from the free ions, or how long it takes for the Cl^- ion to move from its minimum energy position in the tripod ion pair into a position suitable for a back site attack on the moving methyl group. These processes can cause measurable deviations of the rates observed in experiments from the predictions by the transition state theory. Moreover, the lack of these information prevents a smooth transition between the two possible pathways in a single expression. However, a basic link between the free ions and the ion pair pathways is possible, if we assume that the passage along each of these two pathways is controlled by the number of ion pairs and free ions in the solution. This assumption implies that the equilibration of the two species is slower than reaction 1 which is unlikely since no barrier has been found to hinder the association of the ions. At least this approach provides an estimate for the KSE at the very beginning of the reaction.

The molar fraction of ion pairs X_{ip} in the equilibrium can be calculated from the association constant K_{A}

$$X_{\mathrm{ip}} = 1 + \frac{1 - \sqrt{1 + 4\,K_{\mathrm{A}}\,c_0}}{2\,K_{\mathrm{A}}\,c_0} \qquad (32)$$

where c_0 is the initial $(CH_3)_3SCl$ concentration, typically in the millimolar range.[13,14,17–19] The effective barrier is the result of weighing the relative transition state energies by the molar fraction of the corresponding reactants.

$$\Delta G^{\ddagger}_{\mathrm{mix}} = X_{\mathrm{ip}}\,\Delta G^{\ddagger}_{\mathrm{ip}} + (1 - X_{\mathrm{ip}})\,\Delta G^{\ddagger} \qquad (33)$$

The influence of the particle densities δG on the calculated values for K_{A}, $\Delta G^{\ddagger}_{\mathrm{ip}}$ and $\Delta G^{\ddagger}$ has to be corrected according to Equation 7. Figure 10 summarises the calculation of $\Delta G^{\ddagger}_{\mathrm{mix}}$ for 1 M $(CH_3)_3SCl$ solution. The formation of ion pairs increases the effective barrier height $\Delta G^{\ddagger}_{\mathrm{mix}}$ in solvent with a low permittivity and decreases it in solvents with a high permittivity. The transition point between the two regions is marked by the intersection of the lines for $\Delta G^{\ddagger}$ and $\Delta G^{\ddagger}_{\mathrm{ip}}$ at a *cmf* value of 0.95 which coincides with that for the formation of ion pairs after the correction for particle densities.

The predicted accelerations χ for a 1 mM and a 10 mM solution of $(CH_3)_3SCl$ are listed in Table 5. The comparison of the data for $\chi_{1\mathrm{mM}}$ and $\chi_{10\mathrm{mM}}$ shows that the formationof ion pairs reduces the KSE, however this effect diminishes as the temperature increases or the concentration decreases. At 373 K, the predictions for χ suggest that the reaction proceeds entirely *via* free ions in agreement with the calculated values for X_{ip} in water 0.1% and ethanol 2.0% for a 10 mM solution.

T	exp	χ_{fi}	χ_{ip}	$\chi_{1\mathrm{mM}}$	$\chi_{20\mathrm{mM}}$	$\chi_{1\mathrm{M}}$
373.15	6.0	3.589	1.382	3.582	3.473	2.299
298.15	—	4.981	1.494	4.526	2.228	1.389

Table 6 Acceleration factor χ (Equation 31) for ethanol realtive to methanol. T: temperature in K, exp: experimental value calculated from ref.[62], χ_{fi}: $\Delta G^{\ddagger} = G^{\ddagger} - G_{\mathrm{free}}$ (Equation 22), χ_{ip}: $\Delta G^{\ddagger}_{\mathrm{ip}} = G^{\ddagger} - G_{\mathrm{ip}}$ (Equation 25), $\chi_{1\mathrm{mM}}$: Equation 33 at c_0 = 1 mM, $\chi_{20\mathrm{mM}}$: Equation 33 at c_0 = 20 mM, $\chi_{1\mathrm{M}}$: Equation 33 at c_0 = 1 M.

Table 6 summarises the data for the KSE for reaction 1 in methanol and ethanol. The initial $(CH_3)_3SCl$ concentration was 20 mM and the reported rate constant were extrapolated to 100° C. At this temperature, only 4.3% of the salt forms an ion pair in ethanol and 1.4% in methanol. The calculated acceleration factor for a 20 mM solution $\chi_{20\mathrm{mM}}$ of 3.5 is therefore similar to that for a reaction starting from ions at an infinite separation with χ_{fi} being 3.6. Both values compare well to the experimental value of 6.0. However, the data in Table 6 also show that elevated temperatures and low concentrations used in kinetic experiments aggravate the detection of ion pairs in kinetic experiments.

5 Discussion

Early reports[12] on the conversion of trimethylsulfonium salts found reaction 1 to be of first order with hardly any anion effect from CO_3^{2-}, Br^- and Cl^-. This result was refuted by

experiments[13] on the conversion of $(CH_3)_3SClO_4$ in 90% acetone at 373 K. No hydrogen ion was liberated at a signficant rate until LiCl was added to the reaction mixture. The Cl^- ion was consumed rapidly with second order kinetics in agreement with the computational analysis. The calculations also show that a frontside attack of the Cl^- ion in ion pairs does not contribute to the overall reaction despite the proximity of the Cl^- ion and the moving CH_3 group.

The conversion of $(CH_3)_3SClO_4$ in water at 158° C is of first order with no anion effect. The ClO_4^- ion is a very weak nucleophile so that a solvolysis pathway *via* CH_3ClO_4 appears to be unlikely. Also, the analysis of the formation of CH_3^+ ions suggest that the reaction proceeds *via* an attack of the solvent molecule on the $(CH_3)_3S^+$ ion similar to reaction 14. The overall reaction appears to be of pseudo-first order due to the vast excess of solvent molecules rather than standard S_N1 linked to the formation of methyl cations.

A first order reaction is also possible in solvents with a low permittivity due to the formation of ion pairs. Experiments[13,21] suggest that ion pairs become important in solvents with a permittivity lower than 30 in agreement with the calculated value of 28. Moreover, the value of ΔG_{tri} for the formation of ions pairs in water agrees within 1 kcal mol^{-1} with the experimental value[21] for the formation of $[(CH_3)_3S^+ \cdot I^-]$ calculated from the association constant K_A of 6.6 L/mol. Below a threshold permittivity of 30, first order kinetics are caused by the formation of ion pairs rather than the formation of CH_3^+ ions.

The formation of ion pairs increases the effective barrier for the conversion reaction in solvents with a low permittivity and decreases it in solvent with a high permittivity. However, the height of effective barrier decreases continuously as polarity of the solvent decreases, which can be linked to the relative destabilisation of the ions in these solvents. The KSE appears to be driven by solute-solvent interactions and to be hampered by the formation of ion pairs.

The situation is more complicated in solvents with an intermediate permittivity where reaction 1 can proceed *via* ion pairs and free ions simultaneously (Scheme 2). Standard kinetic experiments cannot assign the contribution of each path to the overall reaction,[62] but the comparison of the measured KSE with that obtained from calculations can be used to collect these information. The calculated KSE of 3.5 agrees well with the generally reported[62] fivefold speed up for $(CH_3)_3SX$ with X^- being CN^-, SCN^-, N_3^- and Cl^-. The comparatively large acceleration factor χ of 3.5 agrees much better with that for reaction 1 starting from free ions (χ_{fi} = 3.6) than with that for a pathway stating from ion pairs (χ_{ip} = 1.4). Free ions dominate the reaction, because the ion pairs dissociate at the low concentrations and high temperatures typically used for kinetic experiments. A KSE similar to χ_{ip} can only be expected for very high reactant concentrations and low temperatures.

The used computational model does not contain explicit solute-solvent interactions[63,64] which limits its application to real systems. However, the comparison of the changes in the electron density of the transition states caused by different chemical environments suggests that the PCM covers the important electronic effects despite its simplicity. Moreover, water, methanol and ethanol are nucleophiles by themselves (Equation 2) and hence a change in solvent is always associated with a change of the attacking nucleophile. The quantum chemical calculations suggest, in agreement with experimental data,[62] that the solvolysis of $(CH_3)_3SCl$ is kinetically hindered, but it might be non-neglible with other sulfonium salts. Therefore, it seems to be advisable to use DMSO, nitromethane and acetone to study the KSE experimentally. The *cmf* of these solvents is similar to water-ethanol pairs (Table 1) and the difference between calculated values for χ_{fi} and χ_{ip} is large enough to avoid any ambiguities caused by experimental uncertainties.

The presented analysis is greatly simplified by the relative instability of the CH_3^+ ion, but the moving alkyl group is a *t*-butyl or benzyl group in many kinetic studies. The resonance stabilisation of these cations makes contributions from an S_N1 pathway similar to reaction 8 more likely and the kinetic model for the calculation of the KSE needs to be augmented accordingly.

6 Conclusions

The conversion of $(CH_3)_3SCl$ is analysed with PCM-M05/6-311+G(2d,p) calculations for various solvents with a special emphasis on the role of ion pairs in the mechanism. The calculations reproduce the known thermodynamic and kinetic data of the conversion and related reactions well. The KSE for the conversion reaction indicates that the reaction proceeds *via* free ions instead of ion pairs in methanol and ethanol at 373K despite the medium permittivity of the solvents.

Standard kinetic experiments alone cannot quantify the contribution from ions pairs and free ions to the overall reaction in solvents with an intermediate permittivity. The comparison of the calculated KSE with that from experiments provides these data. The assignment will be much more decisive if the solvent cannot interact with analysed reaction and if the KSE is measured at several temperatures.

Acknowledgement

This work was supported by the Ministry of Science and Technology (MOST) of the Republic of China under Grant numbers NSC 100-2113-M-007-008-MY3 and MOST 103-2113-M-007-012. T.L. acknowledges a university research associateship from the National Tsing Hua University.

References

1 M. J. Hatch, *J. Org. Chem.*, 1969, **34**, 2133–2137.
2 B. Byrne and L. M. L. Lawter, *Tetrahedron Lett.*, 1986, **27**, 1233–1236.
3 P. E. Newallis, J. D. Macke, K. G. Steinbeck and D. N. Wasleski, *Method to prepare trimethylsulfonium halides*, **1990**, Patent US 4978795.
4 P. E. Newallis, J. D. Macke, K. G. Steinbeck and D. N. Wasleski, *Method to prepare trimethylsulfonium halides*, **1992**, Patent US 5118842.
5 E. J. Smutny, S. B. Soloway, L. C. Dowding and J. V. Overbeek, *Method for preventing undesired plant growth*, **1963**, Patent US 3101265.
6 Q. M. Anstee and C. P. Day, *J. Hepatol.*, 2012, **57**, 1097–1109.
7 J. Sarris, N. Schoendorfer and D. J. Kavanagh, *Nutr. Rev.*, 2009, **67**, 125–131.
8 A. Fiecchi, *Double salts of S-adenosil-L-methionine*, **1976**, Patent US 3954726.
9 A. Fiecchi, *Sulphonic acid salts of S-adenosilmethionine*, **1977**, Patent US 4057686.
10 P. B. Deshpande, U. P. Senthilkumar and S.Ganesan, *Stable salts of S-adenosyl-L-methionine (SAMe) and the process for their preparation*, **2003**, Patent US 6649753 B2.
11 N. Buckley and N. J. Oppenheimer, *J. Org. Chem.*, 1994, **59**, 5717–5723.
12 J. L. Gleave, E. D. Hughes and C. K. Ingold, *J. Chem. Soc.*, 1935, 236–244.
13 C. G. Swain and L. E. Kaiser, *J. Am. Chem. Soc.*, 1958, **80**, 4089–4092.
14 C. G. Swain, W. D. Burrows and B. J. Schowen, *J. Org. Chem.*, 1968, **33**, 2534–2536.
15 C. G. Swain and E. R. Thornton, *J. Org. Chem.*, 1961, **26**, 4808–4809.
16 M. N. Islam and K. T. Leffek, *J. Chem. Soc., Perkin Transactions 2*, 1977, 958–962.
17 J. B. Hyne, *Can. J. Chem.*, 1961, **39**, 1207–1213.
18 J. B. Hyne and J. W. Abrell, *Can. J. Chem.*, 1961, **39**, 1657–1669.
19 J. B. Hyne and J. H. Jensen, *Can. J. Chem.*, 1962, **40**, 1394–1398.
20 J. B. Hyne and J. H. Jensen, *Can. J. Chem.*, 1963, **41**, 1679–1685.
21 A. L. Jacobson and J. B. Hyne, *J. Am. Chem. Soc.*, 1960, **82**, 2418–2421.
22 G. D. Markham and C. W. Bock, *J. Phys. Chem.*, 1993, **97**, 5562–5569.
23 G. D. Markham and C. W. Bock, *Struct. Chem.*, 1996, **7**, 281–300.
24 O. Kikuchi, Y. Sano, O. Takahashi and K. Morihashi, *Heteroat. Chem.*, 1996, **7**, 273–279.
25 L. C. Dickinson, D. B. Chesnut and L. D. Quin, *Mag. Reson. Chem.*, 2004, **42**, 1037–1041.
26 National Institute of Standards and Technology, *NIST Computational Chemistry Comparison and Benchmark Database, NIST Standard Reference Database Number 101, Release 15b, August 2011, Editor: Russell D. Johnson III*. `http://cccbdb.nist.gov/`
27 M. J. Frisch *et al.*, *Gaussian 09*, Rev. B.01, 2010.
28 Y. Zhao, N. E. Schultz and D. G. Truhlar, *J. Chem. Phys.*, 2005, **123**, 161103–161106.
29 VMD is developed with NIH support by the Theoretical and Computational Biophysics group at the Beckman Institute, University of Illinois at Urbana-Champaign. `http://www.ks.uiuc.edu/Research/vmd/`
30 J. Cioslowski, *J. Am. Chem. Soc.*, 1989, **111**, 8333–8336.
31 F. De Proft, C. Van Alsenoy, A. Peeters, W. Langenaeker and P. Geerlings, *J. Comp. Chem.*, 2002, **23**, 1198–1209.
32 J. P. Foster and F. Weinhold, *J. Am. Chem. Soc.*, 1980, **102**, 7211–7218.
33 A. E. Reed and F. Weinhold, *J. Chem. Phys.*, 1983, **78**, 4066–4073.
34 A. E. Reed, R. B. Weinstock and F. Weinhold, *J. Chem. Phys.*, 1985, **83**, 735–746.
35 A. E. Reed and F. Weinhold, *J. Chem. Phys.*, 1985, **83**, 1736–1740.
36 J. Tomasi, B. Mennucci and R. Cammi, *Chem. Rev.*, 2005, **105**, 2999–3093.
37 G. Scalmani and M. J. Frisch, *J. Chem. Phys.*, 2010, **132**, 114110–114124.
38 D. W. Tondo, J. R. Pliego, Jr., *J. Phys. Chem. A*, 2005, **109**, 507–511.
39 P. V. Rysselberghe, *J. Phys. Chem.*, 1932, **36**, 1152–1155.
40 T. Lankau and C.-H. Yu, *J. Chem. Phys.*, 2013, **138**, 214102–214112.
41 A. Lewis, J. A. Bumpus, D. G. Truhlar and C. J. Cramer, *J. Chem. Educ.*, 2004, **81**, 596–604.
42 O. Konrad and T. Lankau, *J. Chem. Educ.*, 2007, **84**, 864–869.
43 G.Schaftenaar and J.H. Noordik, *J. Comput.-Aided Mol. Design*, 2000, **14**, 123–134.
44 M. Jannin, R. Pugét, C. de Brauer and R. Perret, *Acta Cryst.*, 1991, **C47**, 982–984.
45 R. W. Bost and J. E. Everett, *J. Am. Chem. Soc.*, 1940, **62**, 1752–1754.
46 J. C. R. Reis, T. P. Iglesias, G. Douhéret and M. I. Davis, *Phys. Chem. Chem. Phys.*, 2009, **11**, 3977–3986.
47 G. Åkerlöf, *J. Am. Chem. Soc.*, 1932, **54**, 4125–4139.
48 S. Weerasinghea and P. E. Smith, *J. Chem. Phys.*, 2003, **118**, 10663–10670.
49 H. Maskill, *The Physical Basis of Organic Chemistry*, Oxford University Press, Oxford, 1st edn, 1989.
50 G. S. Hammond, *J. Am. Chem. Soc.*, 1953, **77**, 334–338.
51 K. Wiberg, *Tetrahedron*, 1968, **24**, 1083–1096.
52 R. F. Nalewajski and P. Gurdek, *Struct. Chem.*, 2012, **23**, 1383–1398.
53 J. March, *Advanced Organic Chemistry*, Wiley Interscience, New York, 3rd edn, 1985.
54 R. A. Sneen, G. R. Felt and W. C. Dickason, *J. Am. Chem. Soc.*, 1973, **95**, 638–639.
55 A. M. Rebollar-Zepeda and A. Galano, *Int. J. Quant. Chem.*, 2012, **112**, 3449–3460.
56 D. H. Ripin and D. E. Evans, *pKa's of Inorganic and Oxo-Acids*. `http://evans.harvard.edu/pdf/evans_pKa_table.pdf`
57 E. A. Moelwyn-Hughes, *Proc. R. Soc. Lon. A*, 1953, **220**, 386–396.
58 M. H. Abraham, D. J. McLennan, *J. Chem. Soc., Perkin Trans. 2*, 1977, 873–879.
59 H. Yamataka, M. Aida, *Chem. Phys. Let.*, 1997, **289**, 105–109.
60 M. Aida, H. Yamataka, M, Dupuis, *Chem. Phys. Let.*, 1998, **292**, 474–480.
61 G. M. Barrow, *Physikalische Chemie*, Friedrich Vieweg & Sohn, Braunschweig, 6th edn, 1984.
62 Y. Pocker and A. J. Parker, *J. Org. Chem.*, 1966, **31**, 1526–1531.
63 A. J. Orr-Ewing, *Nature Chemistry*, 2012, **4**, 522–523.
64 R. Otto, J. Brox, S. Trippel, M. Stei, T. Best and R. Wester, *Nature Chemistry*, 2012, **4**, 534–538.